BMC Complementary Medicine and Therapies

RESEARCH

Open Access

Exploring the potential mechanism of *Radix Bupleuri* in the treatment of sepsis: a study based on network pharmacology and molecular docking

Hao Wang[1], Wei Xiong[2], Yongchu Laram[1], Li Hu[2], Wu Zhong[2*] and Yingchun Hu[2*]

Abstract

Aim To explore, using network pharmacology and RNA-seq technologies, potential active targets and mechanisms underpinning *Radix Bupleuri's* effectiveness during sepsis treatment.

Methods Following the Sepsis-3.0 criteria, the research cohort, comprising 23 sepsis patients and 10 healthy participants, was obtained from public databases. Peripheral blood samples were collected and subjected to RNA-seq analysis. Active ingredients and potential targets of *Radix Bupleuri* were identified using the Bioinformatics Analysis Tool for Molecular mechANism of Traditional Chinese Medicine 2.0 (BATMAN-TCM 2.0) database and TCMSP database. Subsequently, protein-protein interaction (PPI) network construction, Gene Ontology (GO) analysis, and Kyoto Encyclopedia of Genes and Genomes (KEGG) pathway enrichment analysis were conducted to explore cross-targets between disease and drugs. Survival analysis of key targets was performed using the GSE65682 dataset, and single-cell RNA-seq was employed for cellular localization analysis of key genes. Finally, molecular docking and Molecular dynamics simulation of the core target was conducted.

Results Differential expression analysis revealed 4253 genes associated with sepsis. Seventy-six active components and 1030 potential targets of *Radix Bupleuri* were identified. PPI, GO, and pathway enrichment analyses indicated involvement in the regulation of transmembrane transport, monatomic ion transport, and MAPK signaling. Survival curve analysis identified *PIK3CD*, *ARRB2*, *SUCLG1*, and *SPI1* as key targets associated with lower mortality in the high expression group, while higher mortality was observed in the high *PNP* and *FURIN* expression groups. Single-cell RNA sequencing unveiled the cellular localization of PIK3CD, PNP, SPI1, and FURIN within macrophages, while ARRB2 and SUCLG1 exhibited localization in both macrophages and T-cells. Subsequent molecular docking and Molecular dynamics simulation indicated a potential binding interaction for Carvone-PIK3CD, Encecalin-ARRB2, Lauric Acid-SUCLG1, Pulegone-FURIN, Nootkatone-SPI1, and Saikogenin F-PNP.

*Correspondence:
Wu Zhong
zhongwu2876@sina.com
Yingchun Hu
Huyingchun913@swmu.edu.cn

Full list of author information is available at the end of the article

Conclusion *Radix Bupleuri* could modulate immune function by affecting PIK3CD, ARRB2, SUCLG1, FURIN, SPI1, and PNP, thereby potentially improving the prognosis of sepsis.

Keywords Radix Bupleuri, Network pharmacology, RNA-seq, Molecular docking, Sepsis

Introduction

Sepsis represents a life-threatening organ dysfunction resulting from a dysregulated host response to infection [1]. Its intricate development involves complex pathophysiological mechanisms, including inflammatory imbalance, immune system dysfunction, mitochondrial impairment, coagulopathy, abnormal neuroendocrine immune network, endoplasmic reticulum stress, and autophagy [2]. Currently, specific and effective treatments for sepsis are lacking. Nevertheless, research on Traditional Chinese Medicine (TCM) in sepsis treatment has shown promising results, indicating that TCM plays a significant role in reducing mortality, inflammatory indicators, and coagulation indicators in sepsis patients [3]. *Radix Bupleuri*, the main component of Baidu Powder, has been employed in TCM for millennia [4], demonstrating various biological activities, including hepatoprotective, neuroprotective, antiviral, antibacterial, antipyretic, anti-inflammatory, and immunomodulatory effects [5]. Notable active ingredients in *Radix Bupleuri* include Carvone, Encecalin, and Lauric Acid, among others.

The emerging field of network pharmacology involves constructing multi-layered networks encompassing disease-phenotype-gene-drug interactions. This holistic approach aids in predicting drug targets and enhancing drug discovery efficiency [6]. The " multiple targets and multiple pathways" advantage of network pharmacology provides a framework for exploring the mechanism of action of traditional Chinese medicines [7]. Given the unclear underlying mechanisms of *Radix Bupleuri* in improving sepsis prognosis, this study aims to elucidate potential targets and mechanisms using network pharmacology, RNA-seq technology, and extensive public databases.The flow chart of the study is shown in Fig. 1.

Methods

Data source

The raw sepsis data (Data No.: CNP0002611) was obtained from the China National GeneBank DataBase (CNGBdb) (https://db.cngb.org/search/project/CNP0002611/). In the Emergency Intensive Care Unit of Southwest Medical University Hospital, venous blood samples were taken from 23 patients who were inpatients due to sepsis between February 2019 and December 2020. Additionally, venous blood samples from 10 healthy participants served as the control group. This dataset adheres to the sepsis-3.0 criteria (infection+ΔSOFA score≥2) jointly published by the Society of Critical Care Medicine (SCCM) and the Intensive Care Medicine Society of Europe (ESICM) in 2016. GSE65682 and prognostic data were downloaded from the Gene Expression Omnibus (GEO) public database for survival analysis. This study followed the Declaration of Helsinki and was approved by the Ethics Committee of the Affiliated Hospital of Southwest Medical University (ky2018029),Clinical Trial No: ChiCTR1900021261, Date of Registration:4 February 2019.

Screening for differentially expressed RNA

Using the online tool iDEP96ADDIN (http://bioinformatics.sdstate.edu/idep96/) [8], a rigorous data quality control process was implemented. Boxplots were employed to verify dataset comparability and reliability. Principal component analysis (PCA) identified and excluded outlier samples. Differential expression analysis, using the DEseq2 method, involved a minimal fold change (FC) of 2 and a false discovery rate (FDR) below 0.05.

Selecting active ingredients and targets of *Radix Bupleuri*

The Bioinformatics Analysis Tool for Molecular mechANism of Traditional Chinese Medicine 2.0 (BATMAN-TCM 2.0) database [9] (http://bionet.ncpsb.org.cn/batman-tcm/index.php/) was utilized to identify active components and potential targets of *Radix Bupleuri*, screening for a component score greater than 20 and a p-value less than 0.05. In addition, the identification of active ingredients and potential targets of *Radix Bupleuri* from the TCMSP database according to Lipinski rules [8]. Subsequently, after removing the duplicate targets of *Radix Bupleuri* and sepsis, intersection genes for diseases and drugs were obtained. A Venn plot (http://www.liuxiaoyuyuan.cn/) was generated to illustrate the intersected genes.

Protein-protein interaction (PPI) analysis

PPI networks enhance our comprehension of protein interactions within cells, revealing mechanisms and modes of regulation. The Search Tool for the Retrieval of Interacting Genes/Proteins (STRING) database (https://www.string-db.org), built on public databases and literature [10], was utilized for PPI analysis. The organism selected was "homo", and the minimum interaction value was set to 0.7, with concealed disconnected nodes. The resulting intersection genes were imported into the web platform to construct PPI networks.

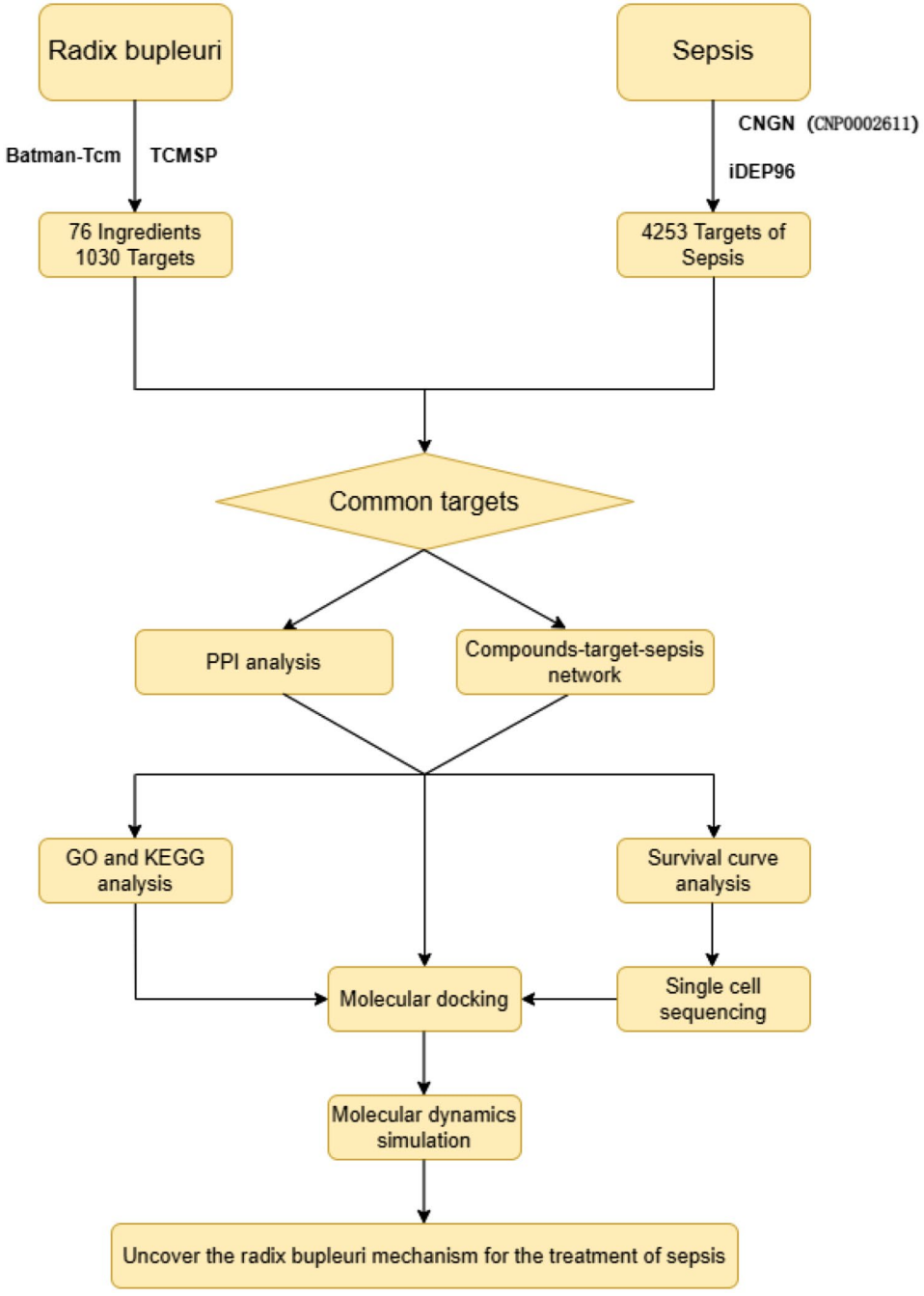

Fig. 1 Flowchart of this study. This figure illustrates the study's workflow, employing network pharmacology and RNA-seq technology to explore *Radix Bupleuri's* potential active targets and mechanisms in the context of sepsis treatment

Construction of "active ingredient - target - disease" network

To further elucidate the mechanism of *Radix Bupleuri* in treating sepsis, network maps of active ingredient targets for sepsis treatment were constructed using Cytoscape 3.7.2. Freedom analysis was performed using its plugin Network Analyzer. The node size in the network was positively correlated with degrees of freedom, and more connections of nodes indicated higher degree values.

Functional enrichment analysis

Metascape (http://metascape.org/) [11] was employed as a gene function annotation analysis tool for Gene Ontology (GO) and Kyoto Encyclopedia of Genes and Genomes (KEGG) enrichment analysis. GO annotation was divided into three categories: molecular function, cellular component, and biological process. KEGG pathway information for different species was also included. Screening was performed with a significance level of

$P \leq 0.01$, and critical gene-disease-signaling pathway networks were constructed with Cytoscape 3.7.2 for visualization.

Survival curve

Survival curve analysis was employed to assess the clinical significance of key targets, exploring their potential prognostic value. The public dataset GSE65682 [12], containing peripheral blood samples from 478 sepsis patients, along with gene expression profiling and clinical 28-day outcome data, was downloaded. Gene expression values were ranked from high to low, dividing the cohort into a low-expression group ($n=293$) and a high-expression group. The log-rank test was used for statistical analysis, and p-values of less than 0.05 were regarded as statistically significant.

Single-cell sequencing

To further elucidate the cell lineage localization of key genes in peripheral blood mononuclear cells (PBMCs), Five peripheral blood mononuclear cells (PBMCs) were obtained for 10× single-cell RNA sequencing from two healthy participants, one patient with systemic inflammatory response syndrome, and two with sepsis. Data quality control was performed using the Cell Ranger online platform, integrating the Spliced Transcripts Alignment to a Reference (STAR) software for data comparison with the reference genome. Single-cell transcriptome sequencing provided absolute values for each transcribed molecule within a single cell using Unique Molecular Identifiers (UMIs) and cell barcodes. Dimensionality reduction techniques, including the Mutual Nearest Neighbors (MNN) algorithm with the t-distributed Stochastic Neighbor Embedding (t-SNE) technique, were applied. t-SNE was used to display the MNN-based downscaling results and determine the ideal cell population [13].

Molecular docking

Critical proteins identified through the "active ingredient-target-disease" network, PPI analysis, and survival curve analysis were selected for molecular docking with their corresponding active components. An adapted version of the protein-ligand docking software, Autodock Vina 1.2.2, was used to evaluate binding energies and interaction sequences. The three-dimensional conformation of the drug or small molecule was retrieved from the PubChem database [14] (https://pubchem.ncbi.nlm.nih.gov/), while the Protein Data Bank (PDB) database [15] (https://www.rcsb.org/) was used to get protein structures. Both protein and ligand files were prepared and converted to PDBQT format, involving the removal of water molecules and the introduction of polar hydrogen atoms. Each protein's domain was enclosed by a grid box, allowing free movement of the molecule. The docking pocket, characterized by a 30 A × 30 A × 30 A square pocket with grid points spaced 0.05 nm apart, facilitated molecular docking studies using Autodock Vina 1.2.2 (http://autodock.scripps.edu/) to determine the binding energy.

Molecular dynamics simulation

The molecular dynamics simulations were performed using AMBER 20 software [16]. Prior to the simulation, the system was subjected to energy optimization, including the steepest descent method with 2500 steps and the conjugate gradient method with 2500 steps. After the system energy optimization was completed, the system was warmed using 200 ps at a fixed volume and constant rate of warming to slowly increase the system temperature from 0 K to 298.15 K. The NVT (isothermal isobaric) system synthesis simulation was carried out for 500 ps to further distribute the solvent molecules homogeneously in the solvent box at a maintained system temperature of 298.15 K. The system was then simulated using the NVT (isothermal isobaric) system synthesis simulation for 500 ps to further homogeneously distribute the solvent molecules in the solvent box. Finally, the NPT (isothermal isobaric) case was performed for 500 ps of equilibrium simulation for the whole system. Finally, the composite system was subjected to NPT (isothermal isobaric) tethered simulations for 100 ns under periodic boundedness conditions. For the simulations, the non-bond truncation distance was set to 10 Å. The Particle mesh Ewald (PME) method was used to calculate long-range electrostatic interactions [17], the SHAKE method was used for the limitation of the bond lengths of the hydrogen atoms, and Langevin's algorithm was used for the temperature control [18]. The collision frequency γ was set to 2 ps^{-1}. The system pressure was 1 atm, and the integration step was 2 fs, with trajectories saved at intervals of 10 ps were used to save trajectories for subsequent analysis.

Results

Differential screening results

Figure 1 depicts the study's flow chart. Boxplots, volcano plots, and PCA were performed to ensure the reliability and comparability of the dataset. In Fig. 2A-C, we identified 4501 differentially expressed genes, with 2447 RNAs highly expressed and 2054 RNAs lowly expressed in the sepsis group. After removing duplicate and irregular genes, a set of 4253 disease-related genes was obtained.

Exploration of active ingredients and targets of *Radix Bupleuri*

We extracted 67 active ingredients of *Radix Bupleuri* and 938 potential targets from the BATMAN-TCM 2.0 database and 38 active ingredients and 143 potential targets

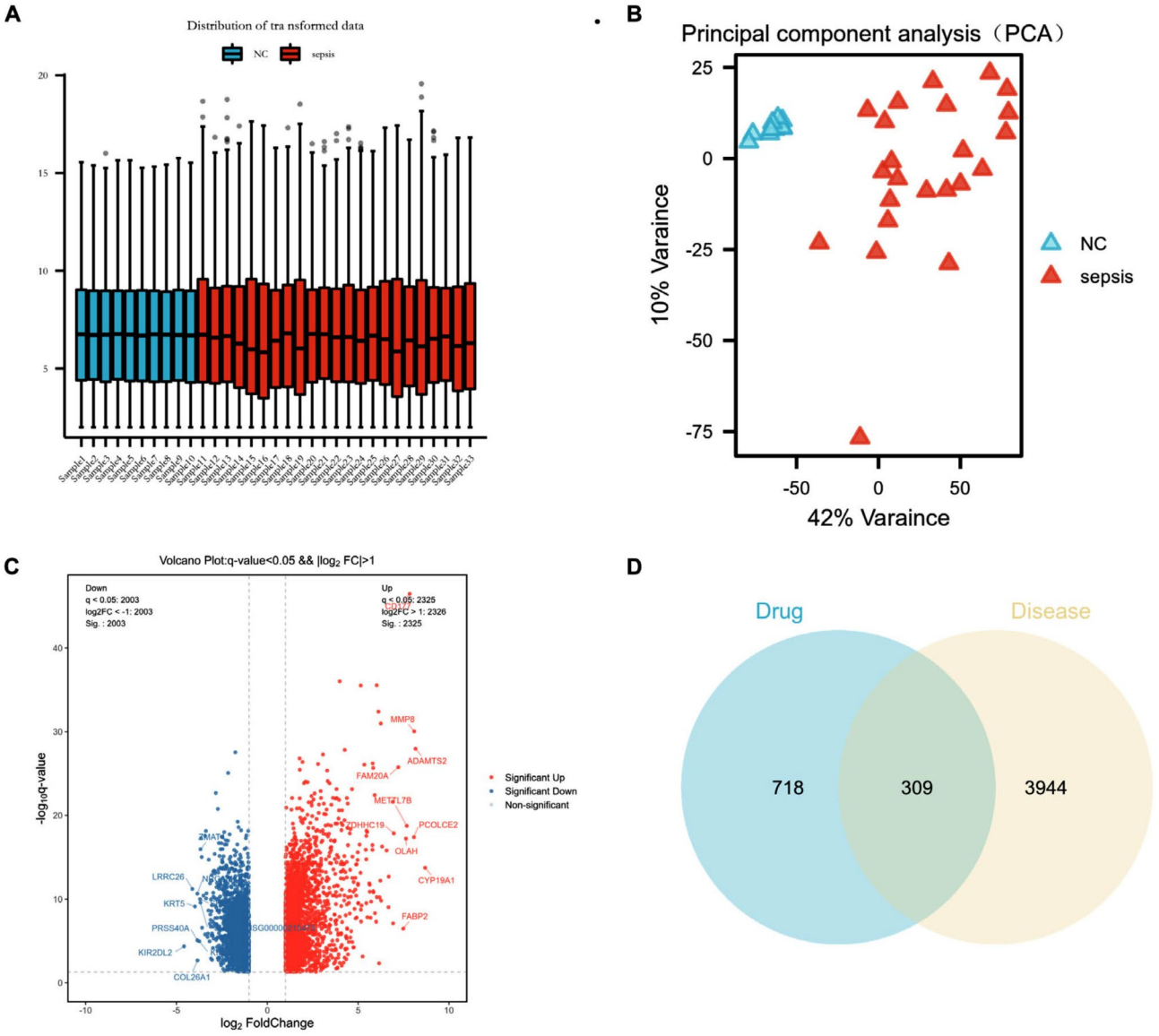

Fig. 2 Performing data quality control, screening differentially expressed genes as well as intersection genes. **A**: The box plots demonstrate uniform data distribution across each sample, ensuring comparability. **B**: PCA reveals significant distinctions between the experimental and control groups, excluding outlier samples. **C**: The volcano plot illustrates downregulated (blue) and up-regulated (red) genes. **D**: Blue represents 1030 drug targets, yellow represents 4253 disease targets, and the central area consists of 309 intersecting genes

of *Radix Bupleuri* from the TCMSP database. After deduplication, a total of 76 active components and 1030 potential targets of *Radix Bupleuri* were identified. A Venn diagram (Fig. 2D) was generated to visualize the overlap between 4253 sepsis targets and 1030 targets associated with the active ingredients of *Radix Bupleuri*, yielding 309 intersected genes. Table 1 depicts these intersected genes along with their corresponding active components and properties.

Construction of "active ingredient - target – disease" network

A network with 309 cross-targets and drug components was generated (Fig. 3) using Cytoscape 3.7.2. Circular nodes represent cross-targets, square nodes represent active pharmaceutical ingredients, and inverted triangle nodes represent diseases. Lines indicate interactions of components with targets. Degrees of freedom analysis using the Network Analyzer plugin revealed that Carvone and Nootkatone exhibited higher values than others among the active compounds, suggesting their potential importance in sepsis treatment.

Table 1 Active ingredients and partial target of Radix Bupleurum

Ingredients	Molecule formula	Molecule weight	Target
Alpha-Linolenic Acid	C18H30O2	278.4	SLC8A1 CKM CKB
Menthyl Acetate	C3H6O2	74.08	NPR1 AR
Saikosaponin	C42H68O13	781	GLRA3 GABRB3
Tetradecane	C14H30	198.39	CAT MIP FBP1
Methyl Palmitate	C17H34O2	270.45	NPR1 TYR
8-Nonenoic Acid	C9H16O2	156.22	APOA2 IL13 IL1
Linolenic Acid	C18H30O2	278.43	APOA2 INS AVP
Beta-Elemene	C8H8O	120.15	DAB2IP CAT
N-Nonanol	C9H20O	144.25	GABRG3 DMTN
Caryophyllene	C15H24	204.35	OXT MIP
Octanoic Acid	C8H16O2	144.21	CHRM1 CHRM2
Saikosaponin V	C53H86O24	1107.2	HDAC2 ITGAL
D-Limonene	C10H16	136.23	NR3C2 IGF1 EDN1
Pentanol	C5H12O	88.15	CNR1 CHRNA4 KCNJ3
Pulsatillic Acid	C30H46O4	470.7	PTGS1 COX1 PTGER1
Sainfuran	C16H14O5	286.28	SREBF1 POR PTPN2
Encecalin	C14H16O3	232.27	RNASE3 YWHAE CALCA
20-Hexadecanoylingenol	C36H58O6	586.94	KIF14 PRKCD CHGA
Stearin	C57H110O6	891.5	NPR2 AR
Lauric Acid	C12H24O2	200.32	COX4I1 COX4I1 SCN4A CES1
Stearic Acid	CH3(CH2)16COOH	284.5	SLC25A1 CES1 COX2
Cubebin	C20H20O6	356.37	TOP2A TUBB
Caprylic Acid	C8H16O2	144.21	OXCT1 PLA2G1B SCN4B
Longifolene	C15H24	204.35	EDN1 IGF1 EDN1
Saikosaponin C	C48H78O17	927.12	DNMT1 POLB DNMT1
Longispinogenin 3-O-Beta-D-Glucuronopyranoside	C36H58O9	634.94	NR3C1
Phenylacetic Acid	C8H7O2-	135.14	SIRT2 CNTF
Linalyl Acetate	C20H36O2	308.5	FADS1 ESR1 FADS1
Octalupine	C15H24N2O2	264.36	DPP4
Saikosaponin D	C42H68O13	780.98	DNMT1POLB
7-Octen-4-Ol	C10H18O	154.25	KL GFI1 BAX

Table 1 (continued)

Ingredients	Molecule formula	Molecule weight	Target
Longispinogenin	C30H50O3	458.72	PGR ADA TFAP2C
Pulegone	C10H16O	152.23	ATM
Stigmasterol	C29H48O	412.7	KCNQ1 ADH1C
Alpha-Spinasterol-Beta-D-Glucoside	C35H58O6	560.9	ATP1A1
Angelicin	C11H6O3	186.16	B4GALT1 GC
Myrtenol	C10H16O	152.23	DHRS4 DHRS4
Tridecanoic Acid	C13H26O2	214.34	BBOX1 AR
Myrtenal	C10H14O	150.22	CRP TSPO
Kaempferol	C15H10O6	286.24	NQO1
Adonitol	C5H12O5	152.15	CHRNA2 KCNJ3 GABRE
3-Methylcyclotridecan-1-One	C14H26O	210.36	TYR
Quercetin	C15H10O7	302.24	DRD3 DRD2
Geraniol	C10H18O	154.25	HSD17B7
Beta-Humulene	C15H24	204.35	KCNQ1 CRLF1
Saikosaponin B	C42H68O13	780.98	GLRA3
Saikosaponin K	C54H88O22	1089.3	GLRA3 GABRB3
Nootkatone	C15H22O	218.33	C5 PHB CRP TNF
Delta-Terpineol	C10H18O	154.25	TRPV3 PGR
Naphthalene	C10H8	128.17	RNASE3 LTA
Spinasterol	C29H48O	412.7	TRIM24 RXRA
Guaiacol	C7H8O2	124.14	SEC14L3 TRPV3
Myrtanol	C10H18O	154.25	VCAM1 GRIA4
Saikogenin F	C30H48O4	472.7	PGR PNP
Carvone	C10H14O	150.22	NR3C1 PIK3CD
Saikosaponin A	C42H68O13	780.98	POLB
Myricadiol	C30H50O2	442.72	VDR PGR
Nonanoic Acid	C9H18O2	158.24	SDHA CES1 COX2
Saikosaponin T	C43H72O14	813.15	POLB DNMT1 ADORA2B
Eugenol	C10H12O2	164.2	OPRK1 CNR1

Table 1 (continued)

Ingredients	Molecule formula	Molecule weight	Target
Saikogenin E	C30H48O3	456.7	MIF ADORA1 ITFG2
Linalool	C10H18O	154.25	TFAP2C PGR TOX3
Undecanoic Acid	C11H22O2	186.29	TRPA1 OPRK1
Myrcene	C10H16	136.23	FBP1 GRIN2A SPARC
Alpha-Limonene	C10H16	136.23	LEP CAT
Thymol	C10H14O	150.22	HRC PDE4B COLQ
(+)-Anomalin	C24H26O7	426.5	KCNH2 STX3
3,5,6,7-tetramethoxy-2-chromone	-	432.46	PTGS2 PTGS1
Areapillin	C18H16O8	360.34	ESR1 CCNA2
Baicalin	C21H18O11	446.39	AR MAOB
Isorhamnetin	C16H12O7	316.28	ACHE RELA
Longikaurin A	C20H28O5	348.48	ESR2 OLR1
Petunidin	C16H13O7+	317.29	NOS2 CHRM2
Troxerutin	C27H30O16	346.56	PTGS1 PGR
α-spinasterol	C29H48O	412.77	CCNA2 NR3C2

PPI analysis

After removing irrelevant data, the PPI network was modified to include 104 nodes. *PIK3CD*, *ARRB2*, *SUCLG1*, *FURIN*, *SPI1*, and *PNP* were situated at the core of the network (Fig. 4A). These genes were associated with mast cell differentiation, small molecule binding, multicellular biological process regulation, and response to organic substances, indicating their potential as important targets for *Radix Bupleuri* in improving the prognosis of sepsis. A heatmap of the expression of these key genes was generated (Fig. 4B).

GO and KEGG enrichment analysis

A comprehensive compilation of 7826 functional gene profiles was obtained based on GO annotation of cross-targets. In this collection, 6217 genes were enhanced in biological processes, 508 in cellular components, and 1101 in molecular functions. GO enrichment analysis revealed that the target was primarily engaged in transmembrane transport regulation, monatomic ion transport, and redox (Fig. 5A). Target genes were primarily engaged in cancer pathways, MAPK signaling pathways, and vascular smooth muscle contraction, according to KEGG pathway analysis (Fig. 5C). To further elaborate the relationship between them, GO and KEGG enrichment analysis results were presented as network graphs, and the networks were displayed by Cytoscape3.7.2, with each node in the GO analysis network representing a term and first colored by its cluster ID (Fig. 5B), with polygons representing key genes, inverted triangles representing signaling pathways(Fig. 6).

Survival curve analysis

To evaluate the association between patient prognosis and the 309 cross-targets, a prognostic analysis was conducted by integrating the public database GSE65682 [12]. The log-rank test demonstrated a significant correlation between prognosis and the expression of *PIK3CD*, *ARRB2*, *SUCLG1*, *FURIN*, *SPI1*, and *PNP* (Fig. 7A-F). The larger the gap between the survival curves, the

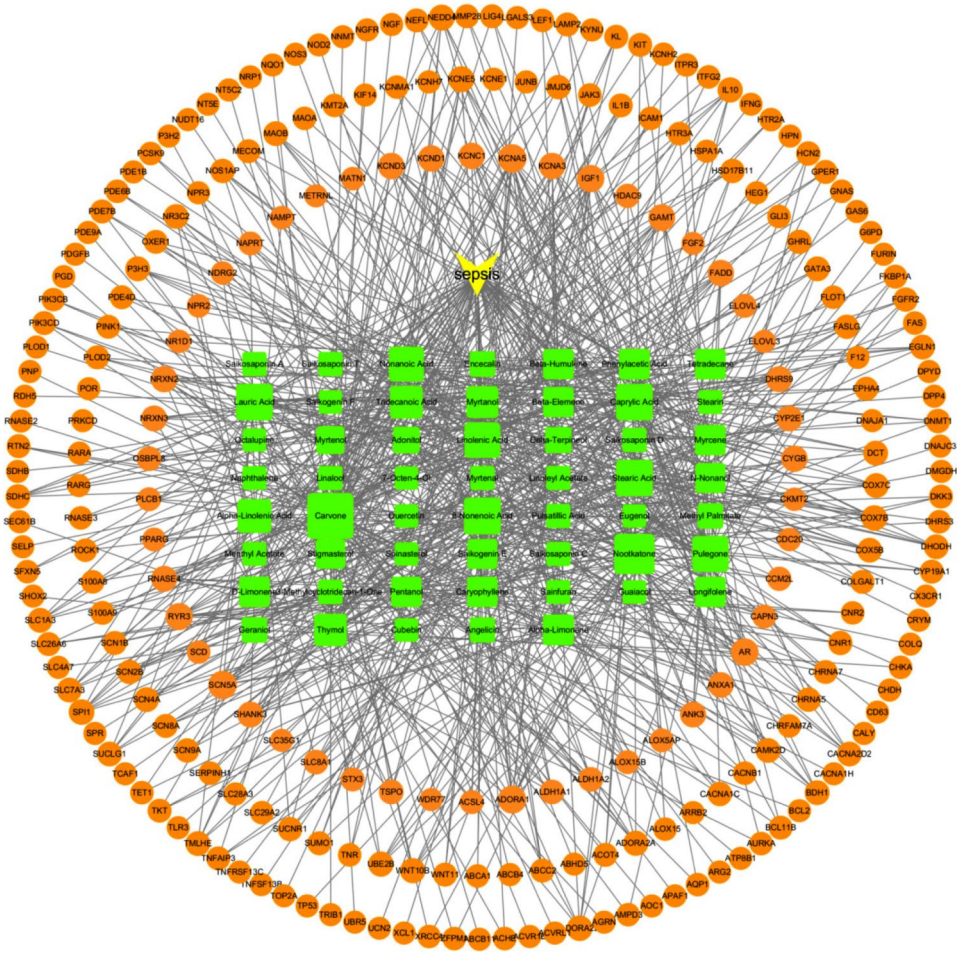

Fig. 3 Drug component target network diagram: In this network, circular nodes represent intersected genes, square nodes indicate active compounds of *Radix Bupleuri*, and inverted triangle nodes indicate diseases. Lines indicate drug interactions with ingredients and targets

more pronounced the change in patient prognosis. High expression of *PIK3CD*, *ARRB2*, *SUCLG1*, and *SPI1* was associated with lower mortality rates, while low expression of *PNP* and *FURIN* indicated a better prognosis. Therefore, *PIK3CD*, *ARRB2*, *SUCLG1*, *FURIN*, *SPI1*, and *ARRB2* are potential core targets for *Radix Bupleuri* in sepsis treatment. Box plots were generated to illustrate the expression levels of these six key genes in normal and sepsis groups (Fig. 8A-F).

Single-cell RNA sequencing

Transcriptome sequencing analysis of the five cell samples (Fig. 9A) incorporated the six key genes identified in this study—*PIK3CD*, *ARRB2*, *SUCLG1*, *FURIN*, *SPI1*, and *PNP*—into the single-cell libraries for cell line localization. The results showed that PIK3CD, PNP, SPI1, and FURIN were predominantly situated in macrophages, while ARRB2 and SUCLG1 was predominantly located in macrophages and T cells (Fig. 9B-I).

Molecular docking

Based on the above analysis, Carvone, Encecalin, Lauric Acid, Pulegone, Nootkatone, and Saikogenin F, the active components of *Radix Bupleuri*, underwent molecular docking studies with PIK3CD, ARRB2, SUCLG1, FURIN, SPI1, and PNP, respectively (Fig. 10A-F). Affinity values below -4.25 kcal·mol^{-1} indicate binding activity, those below -5.0 kcal·mol^{-1} indicate binding solid activity, and values below -7.0 kcal·mol^{-1} indicate significant docking interactions [19]. The results of docking the active components to the targets are summarized in Table 2, with Saikogenin F showing the best docking activity with PNP.

Molecular dynamics simulations

Molecular dynamics results showed that Carvone-PIK3CD, Encecalin-ARRB2, Lauric Acid-SUCLG1, Pulegone-FURIN, Saikogenin F-PNP, and Nootkatone-SPI1 six systems of RMSD, RMSF, RoG, SASA, and hydrogen bonding changes. Except for Nootkatone-SPI1, the RMSD of the five systems showed good convergence during the simulation period, indicating that these

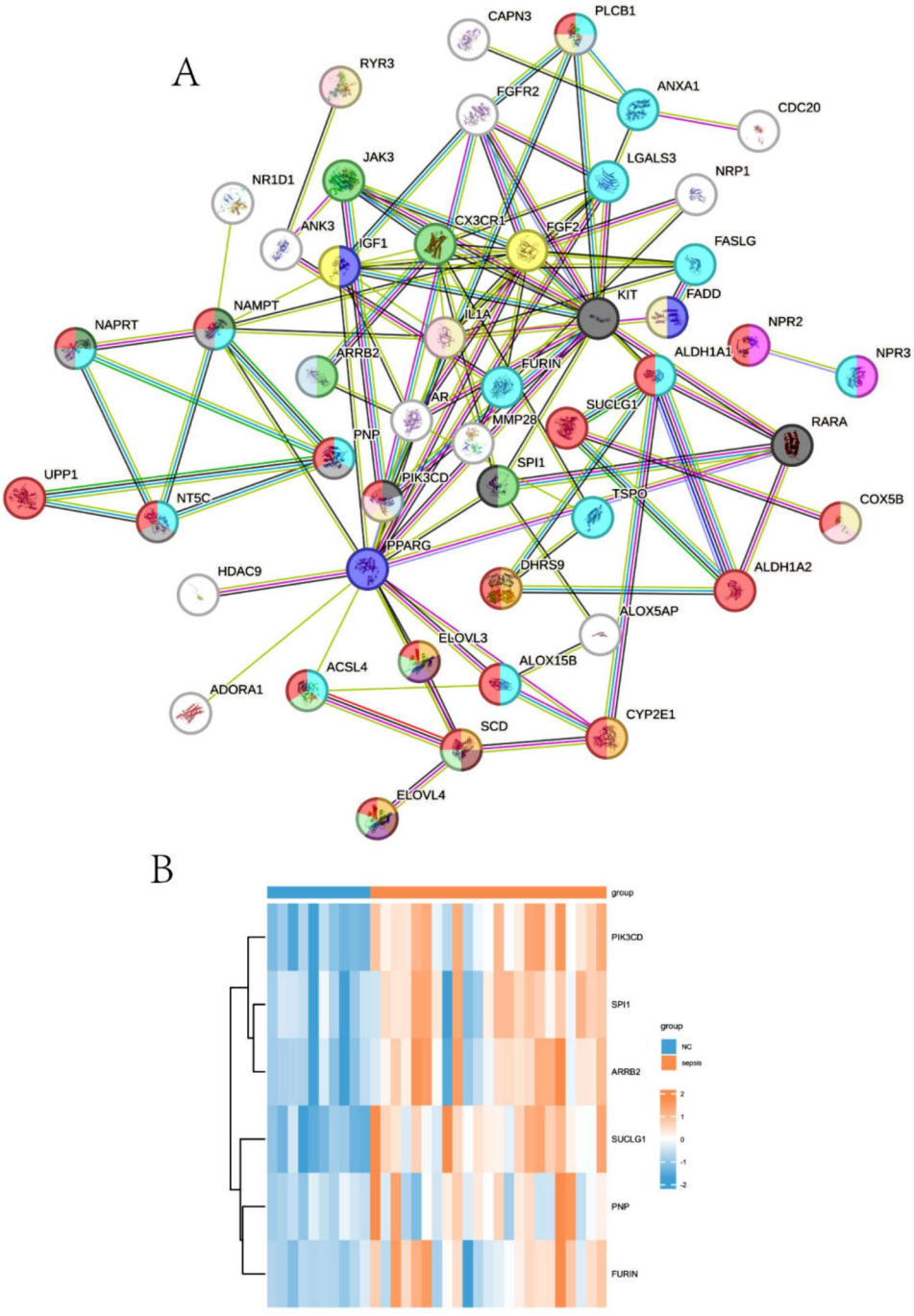

Fig. 4 PPI Analysis and intersected gene analysis. A: The interaction network between proteins. PIK3CD, ARRB2, SUCLG1, FURIN, SPI1, and PNP are located at the center of this network. B: Heatmap of the six key genes at the center of the PPI network (*PIK3CD*, *ARRB2*, *SUCLG1*, *FURIN*, *SPI1*, *PNP*). Blue represents higher expression, and yellow represents lower expression

complexes were dynamically stable and did not undergo major conformational changes; whereas the RMSD of the Nootkatone-SPI1 complex fluctuated considerably during the first 50 ns second simulation period(Fig. 11). The RMSF results showed that the RMSF of the protein after binding small molecules was low except for the ends, indicating that the core structure of the protein possesses better rigidity(Fig. 12A-F). The trend of radius of gyration (RoG) showed that the Carvone-PIK3CD, Lauric Acid-SUCLG1, Pulegone-FURIN, and Saikogenin F-PNP systems had less fluctuation in compactness, and Encecalin-ARRB2, Nootkatone-SPI1 systems fluctuated more(Fig. 13).SASA analysis showed that the fluctuation of solvent-accessible and surface area of the

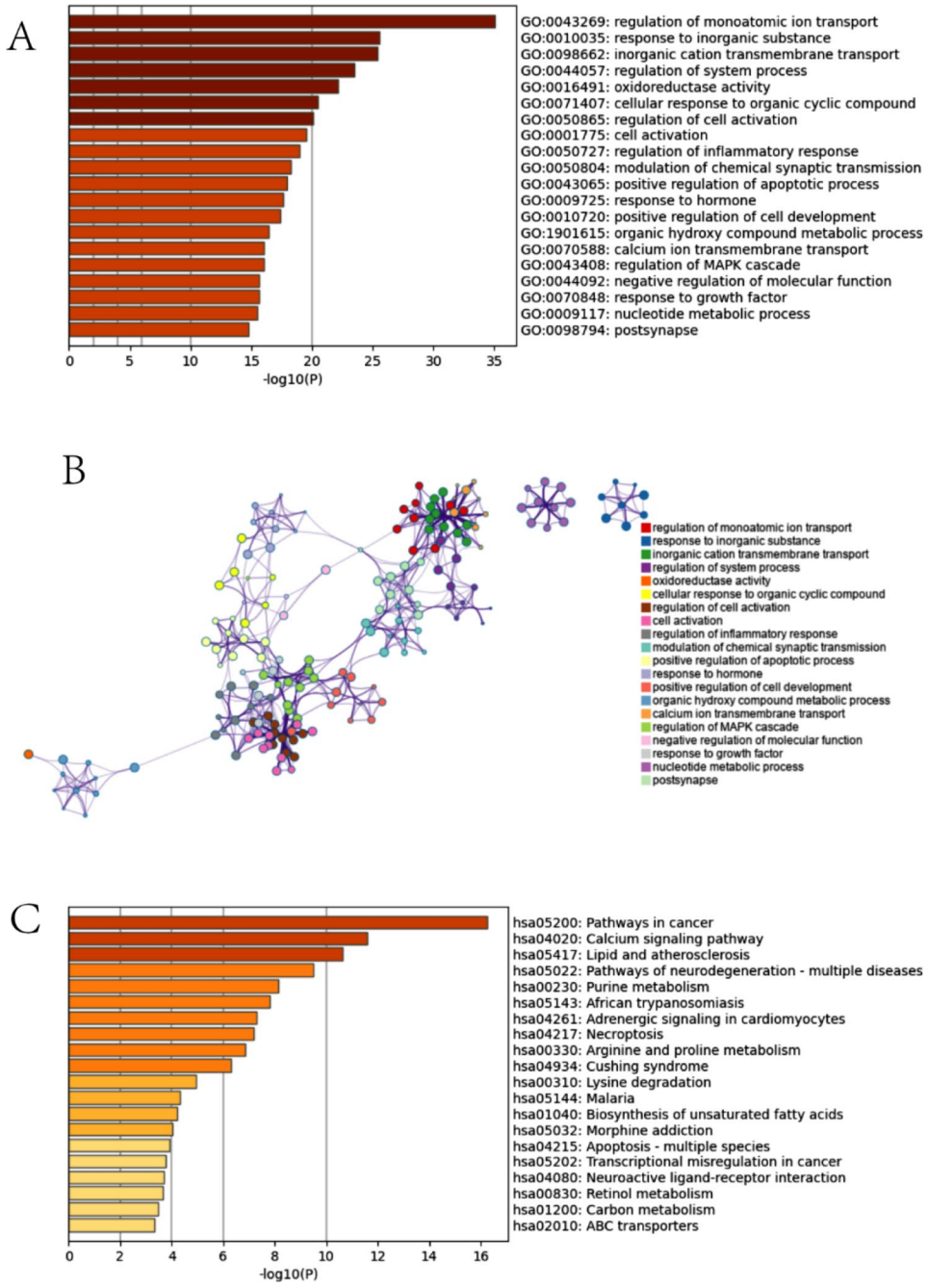

Fig. 5 GO and KEGG enrichment analysis of cross-targets. **A**: GO enrichment analysis revealed that the target was primarily involved in biological processes such as transmembrane transport regulation, monatomic ion transport regulation, and redox. **B**: Different colors of each node correspond to different biological processes. (Cluster ID) **C**: KEGG pathway analysis showed that target genes were primarily associated with various signaling pathways such as cancer pathway, MAPK signaling pathway, and vascular smooth muscle contraction

six systems was smooth, indicating that the complexes existed stably in aqueous solution(Fig. 14). Hydrogen bonding analysis showed that the number of hydrogen bonds of Lauric Acid-SUCLG1 complexes stabilized at 2–3 at the late stage of the simulation, Pulegone-FURIN at 1–2, and the rest of the systems at 0–1, suggesting that hydrogen bonding contributes to the Lauric Acid- SUCLG1 binding contributes the most, followed by Pulegone-FURIN(Fig. 15A-F).

Discussion

Sepsis, characterized by a systemic inflammatory response to infection, remains a leading cause of global mortality [20]. With the lack of specific effective

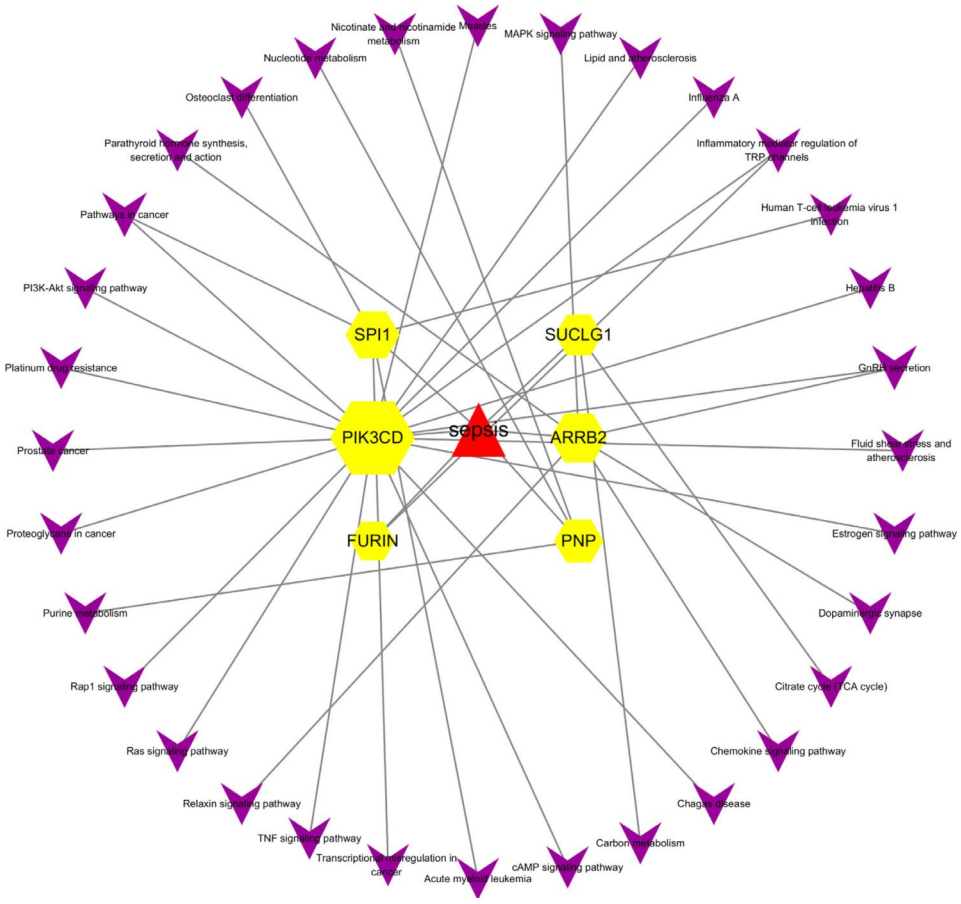

Fig. 6 target-disease-signaling pathway network. Polygons in the "target-disease-signaling pathway" network represent key genes, inverted triangles represent signaling pathways, and rectangles represent diseases

treatments, TCM shows promise in reducing sepsis-induced organ dysfunction through anti-inflammatory actions, oxidative stress reduction, immunity enhancement, and cellular homeostasis maintenance [21]. This study utilized a network pharmacology approach to reveal how the active ingredients of *Radix Bupleuri* modulate immune responses and signaling processes in sepsis patients by interacting with core targets, thereby improving the prognosis of sepsis patients. The resulting PPI network identified 104 targets, with six potential targets selected for further investigation: PIK3CD, ARRB2, SUCLG1, FURIN, SPI1, and PNP. These findings lay the groundwork for future studies on *Radix Bupleuri*'s therapeutic mechanism against sepsis.

ARRB2, a member of the G protein-coupled receptor adaptor family [22], promotes the anti-apoptotic Akt signaling pathway and prevents apoptosis by inhibiting pro-apoptotic ERK1/2 and p38 MAPKs [23]. It also enhances EPC-mediated neovascularization via ERK and Akt signaling pathways [24]. Survival curve analysis indicated higher ARRB2 expression in the group with a better prognosis of sepsis, associated with increased survival. RNA-seq analysis revealed ARRB2's predominant localization in macrophages and T-cell lines. Network pharmacological analysis identified Encecalin, an active component of *Radix Bupleuri*, as a potential antibacterial agent targeting ARRB2.

FURIN, a significant mammalian proprotein convertase, plays a substantial role in the pathophysiology of neurodegenerative diseases and neuropsychiatric disorders [25]. Additionally, FURIN is responsible for the processing of transforming growth factor-beta, elevated in bronchoalveolar lavage fluid of PWCF, associated with neutrophilic inflammation and decreased lung function [26]. In the present study, survival analysis demonstrated reduced FURIN expression in the sepsis group with a better prognosis, leading to increased survival. Accordingly, downregulated FURIN expression may be advantageous in sepsis, and RNA-seq analysis revealed its predominant localization in macrophage cell lines. Network pharmacological analysis highlighted Pulegone, an active ingredient in *Radix Bupleuri*, targeting FURIN and exhibiting antibacterial properties.

Purine nucleoside phosphorylase (PNP) is a vital enzyme involved in purine nucleoside degradation, and PNP deficiency leads to progressive T-cell

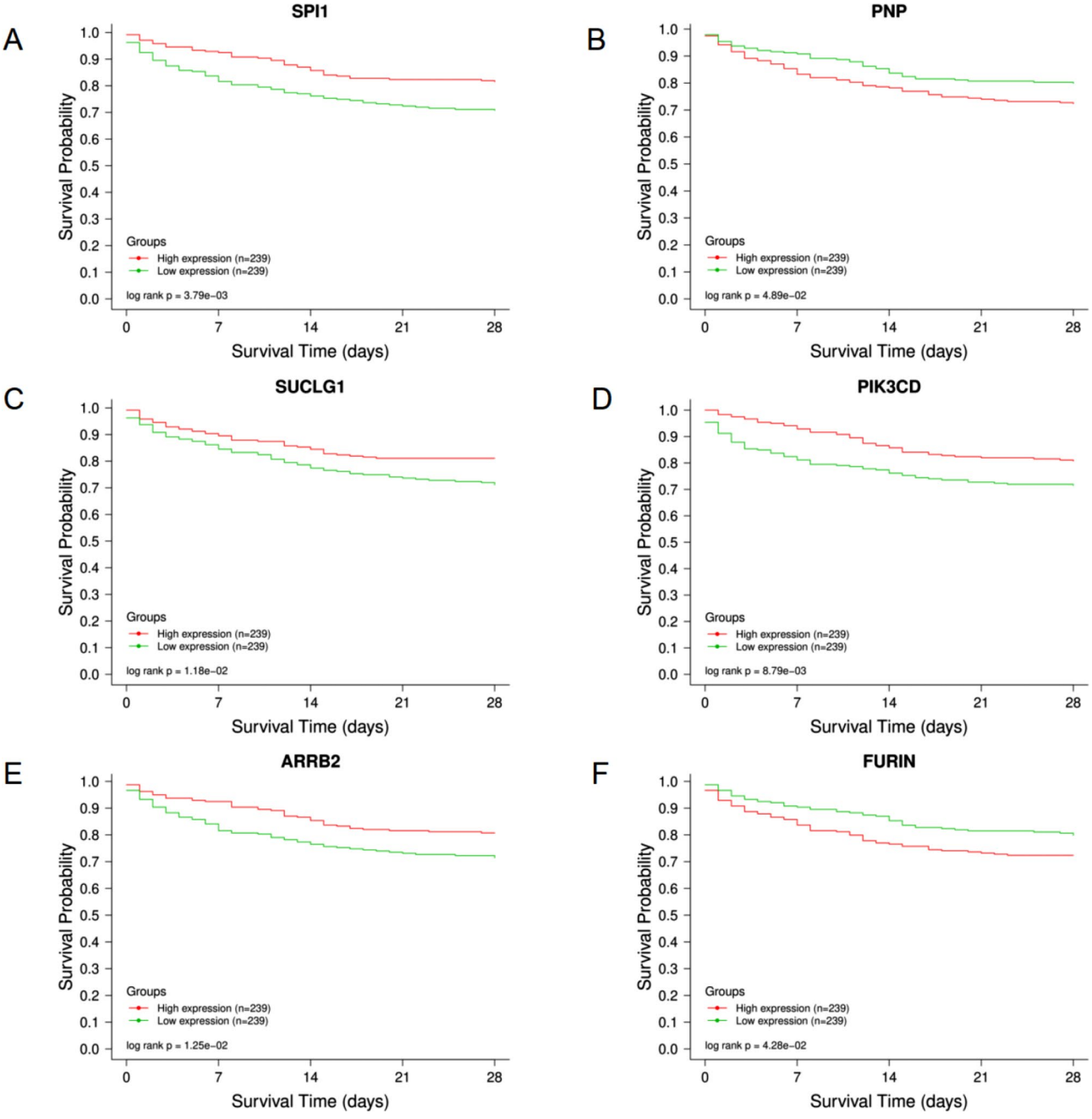

Fig. 7 Survival curve analysis of six key targets. The plot shows survival time in days on the horizontal axis and survival on the vertical axis. Green lines correspond to low mRNA samples, while red lines represent high mRNA samples. **A** – **F**: The lower mortality rates were observed in the high-expression groups of PIK3CD, ARRB2, SUCLG1, and SPI1, and the low-expression groups of PNP and FURIN, indicating a better prognosis ($P < 0.05$)

immunodeficiency, increased susceptibility to infections, autoimmunity, and neurological abnormalities [27]. Mutations in the *PNP* gene can result in decreased T lymphocyte numbers, causing immunodeficiency [28]. In this study, survival analysis indicated decreased PNP expression in the sepsis group with a better prognosis, contributing to increased survival. Reduced PNP expression may favor sepsis, and RNA-seq analysis showed predominant localization in the macrophage lineage. Network pharmacological analysis revealed Saikogenin F, an active ingredient in *Radix Bupleuri*, targeting PNP and exhibiting antibacterial properties.

SUCLG1 is a gene encoding a protein crucial for maintaining mitochondrial nucleotide pool balance [29], and its mutations cause mitochondrial encephalomyopathy [30]. Survival analysis showed increased SUCLG1 expression in the sepsis group with a better prognosis, leading to increased survival. Elevated SUCLG1 expression may

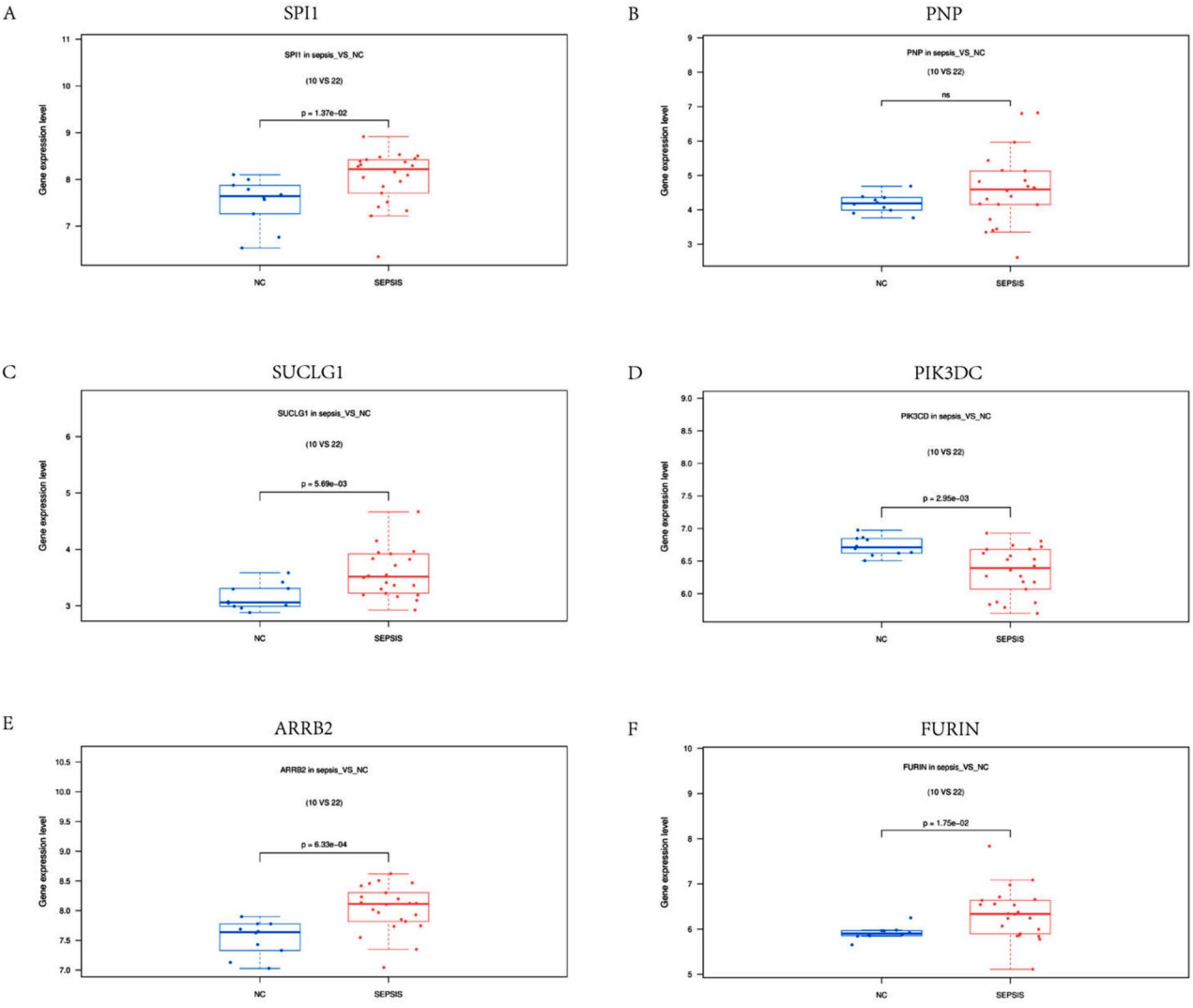

Fig. 8 Expression levels of six key genes. *FURIN*, *ARRB2*, *SUCLG1*, *SPI1*, and *PNP* were highly expressed in the sepsis group. *PIK3CD* expression was low in the sepsis group ($P < 0.05$)

be favorable in sepsis, and scRNA-seq analysis identified its primary location in macrophages and T cells. Network pharmacological analysis uncovered Lauric Acid, an active component in *Radix Bupleuri*, with the potential to target SUCLG1 and exhibit antibacterial properties.

PIK3CD, closely tied to the immune function of the human body, can influence T cell activation, differentiation, and trafficking [31]. Mutations in PIK3CD may result in symptoms such as immunodeficiency and autoimmunity [32]. Survival curve analysis demonstrated increased PIK3CD expression in the sepsis group with a better prognosis, contributing to increased survival. Elevated PIK3CD expression may favor sepsis, and RNA-seq analysis indicated its predominant location in macrophage cell lines. Network pharmacology analysis revealed that Carvone, an active component in *Radix Bupleuri*, targets PIK3CD and exhibits antibacterial properties.

SPI1, a transcription factor, may play a crucial role in leukemogenesis when abnormally regulated [33]. Studies have shown that SPI1 regulates microglia/macrophage orientation and maturation and may affect monocyte autophagy in a mouse sepsis model by regulating ANXA [34, 35]. Survival curve analysis indicated higher SPI1 expression in the sepsis group with a better prognosis, resulting in increased survival. Increased SPI1 expression may be advantageous in sepsis, and RNA-seq analysis revealed its predominant location in macrophage cell lines. Network pharmacological analysis highlighted Nootkatone, an active compound in *Radix Bupleuri*, targeting SPI1 and exhibiting antibacterial properties.

Unlike previous studies on sepsis, this study used single-cell sequencing to better understand the individual differences and pathological mechanisms of sepsis patients. Based on this information, personalized

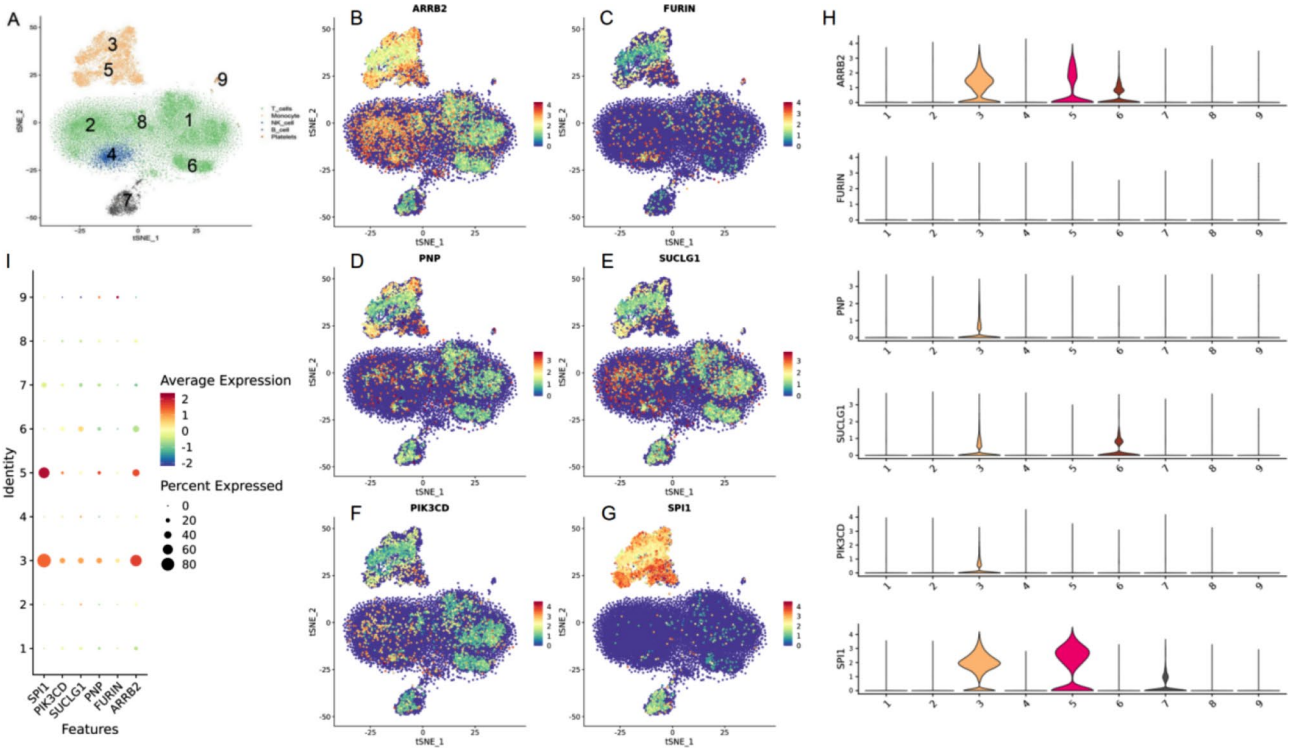

Fig. 9 Cell line localization of key genes. **A**: Groups 3 and 5 represent macrophages, Group 4 represents natural killer cells, and Groups 1, 2, 6, and 8 represent T cells. B cells represent Group 7, and Group 9 represents platelets. **B-H**: PIK3CD, PNP, SPI1, and FURIN were primarily situated in macrophages, SUCLG1and ARRB2 was primarily situated in macrophages and T cells. **I**: Bubble plots show the expression abundance values and proportions of each hub gene in different cell populations

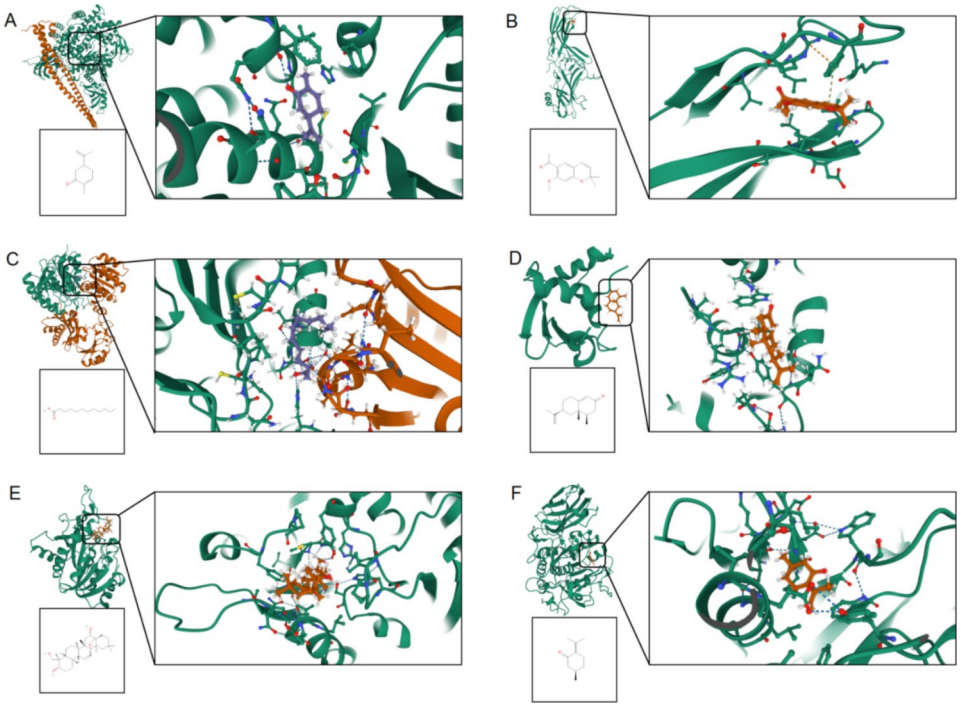

Fig. 10 Molecular docking results. **A**: The binding affinity between Carvone and PIK3CD is -6.258 kcal·mol^{-1}. **B**: The binding affinity between Encecalin and ARRB2 is -6.954 kcal·mol^{-1}. **C**: The binding affinity between Lauric Acid and SUCLG1 is Lauric Acid-SUCLG1. **D**: The binding affinity between Nootkatone and SPI1 is -5.546 kcal·mol^{-1}. **E**: The binding affinity between Saikogenin **F** and PNP is -8.86 kcal·mol^{-1}. **F**: The binding affinity between Pulegone and FURIN is -6.348 kcal·mol^{-1}

Table 2 Molecular docking results

Compounds	Targets	Bind Energy
Encecalin	ARRB2	-6.954kcal·mol^{-1}
Pulegone	FURIN	-6.348kcal·mol^{-1}
Saikogenin F	PNP	-8.86 kcal·mol^{-1}
Lauric Acid	SUCLG1	-5.009kcal·mol^{-1}
Carvone	PIK3CD	-6.258kcal·mol^{-1}
Nootkatone	SPI1	-5.546kcal·mol^{-1}

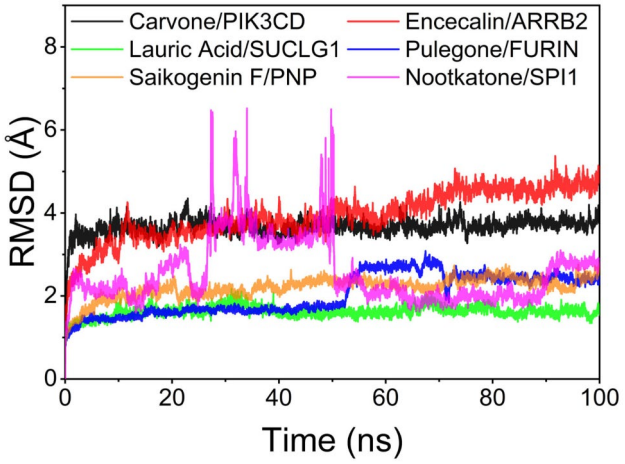

Fig. 11 Root mean square deviation (RMSD) of the complexes during molecular dynamics simulation with time. The root mean square deviation of the molecular dynamics simulation can reflect the movement process of the complex, the larger RMSD as well as the more violent fluctuation indicates the violent movement, and on the contrary, the movement is smooth

therapeutic strategies can be developed to improve treatment efficacy and prognosis. In addition, potential targets of action and signaling pathways of *Radix Bupleuri* were analyzed to support its clinical translation. Molecular docking and molecular dynamics simulations were used to analyze the binding of *Radix Bupleuri* to its targets, revealing new ideas on the pathogenesis of sepsis and providing new avenues for the treatment and prevention of the disease. In summary, this study integrates multiple advanced technologies and has broad prospects for future research and clinical applications.

Based on previous studies, Pulegone has been shown to exert anti-inflammatory effects on LPS-induced sepsis in mice by inhibiting NLRP3 expression [36]. We speculated that Pulegone may modulate FURIN expression in sepsis through a similar mechanism, but whether Pulegone exerts its antisepsis effect by down-regulating FURIN remains unclear. Saikogenin F increases the expression of Bax, cleaved-caspase-3, cleaved-caspase-9, and cleaved-poly ADP-ribose polymerase (PARP) and decreases the expression of Bcl-2, resulting in a significant inhibitory effect on A549 cells, which can be considered as a potential anticancer drug [37]. Similarly, Lauric Acid promotes the expression of mitochondrial biogenesis-regulated genes such as TFAM, PGC-1α, and PPAR-γ, thereby improving insulin sensitivity [38]. Carvone has been shown to express antioxidant and anti-inflammatory capacity by promoting the expression of TNF-α, IL-1β, IL-6 and NF-κB mRNA in rats [39]. Nootkatone was found to attenuate asthmatic airway inflammation by reducing the production of Th2 inflammatory cytokines (IL-4, IL-5, and IL-13) in reduced serum levels of BALF and IgE, and by inhibiting ROS-triggered NLRP3 activation [40]. In addition, Encecalin has also been shown to play a role in controlling blood glucose levels, thus playing a very important role in the therapeutic response of diabetic patients [41]. In summary, these active ingredients have shown positive pharmacological activity in other disease models by acting on targets associated with them. This provides new ideas and targets for the clinical treatment of sepsis. Although we have analyzed through previous studies that these active ingredients (Pulegone, Saikogenin F, Lauric Acid, Carvone, Nootkatone, and Encecalin) may exert their antisepsis effects through the modulation of the relevant genes, direct evidence is still insufficient and the specific mechanisms by which these active ingredients regulate the target genes (PIK3CD, ARRB2, SUCLG1, FURIN, SPI1, and PNP) remains unclear, and the regulatory mechanisms of these genes in different pathological states may have similarities in sepsis, but this hypothesis needs to be verified by further studies.

The study has certain limitations that merit consideration. Firstly, the bioinformatic data available from the public databases relied upon for this study are limited. The sample size involved in this study kind is small, if we want to fully understand the pharmacological effects of *Radix Bupleuri*. A large number of clinical trial validation and evidence-based medical studies are also needed, in addition, the inhibitory or promoting effects of small molecules binding to key targets need to be verified by further mechanistic cellular experiments, which will be carried out in our subsequent studies.

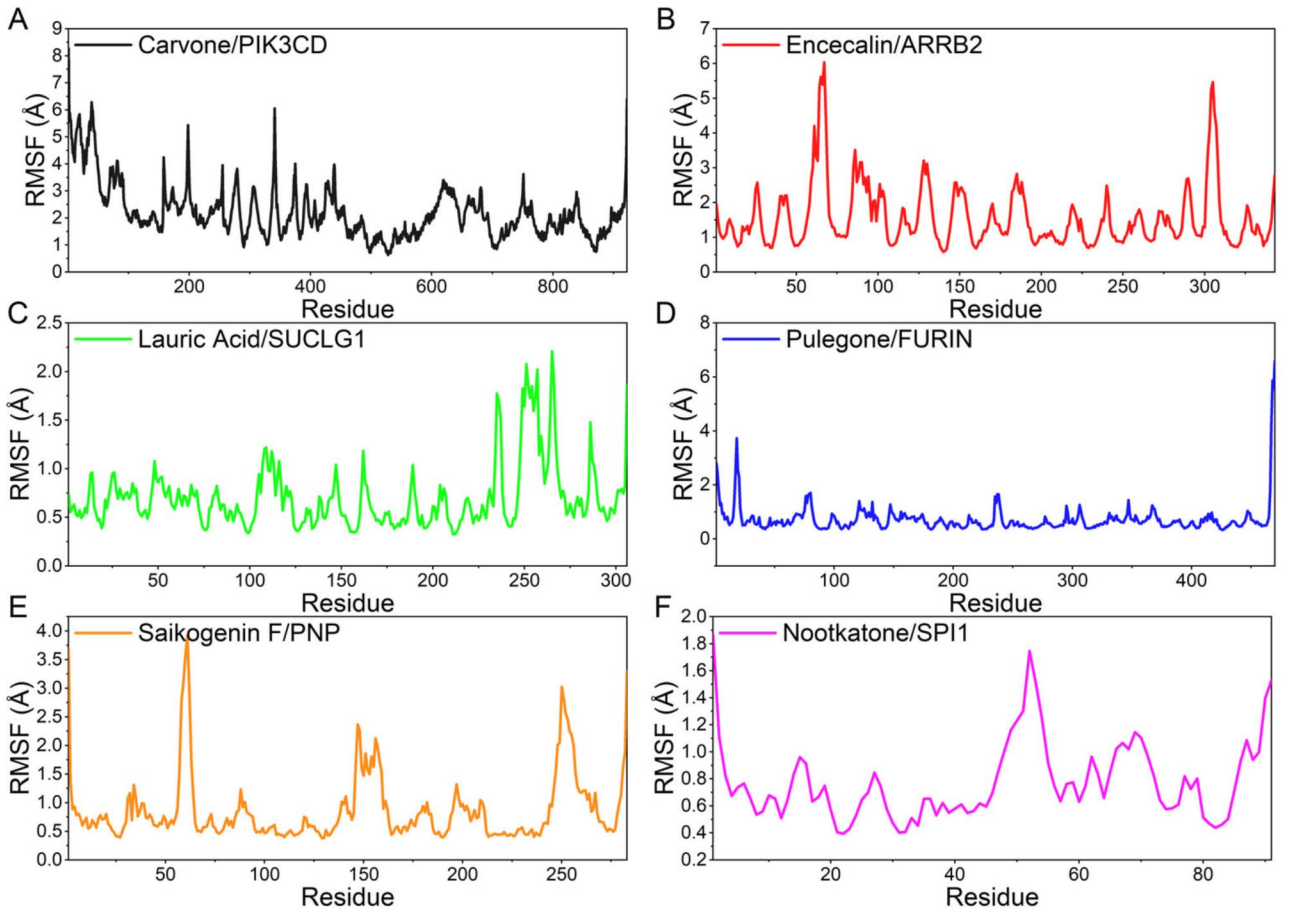

Fig. 12 Root Mean Square Fluctuation (RMSF) calculated based on molecular dynamics simulation trajectory. **A-F**: RMSF can respond to the protein flexibility during molecular dynamics simulation. Usually, the protein flexibility decreases after the drug binds to the protein, which in turn stabilizes the protein while exerting the enzyme activation effect

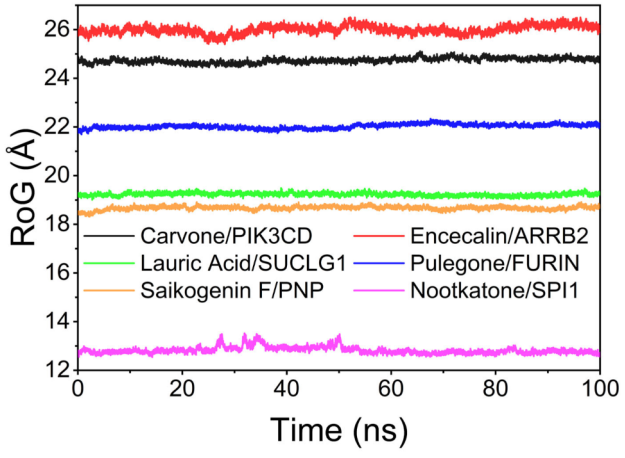

Fig. 13 Radius of gyration of the six systems during molecular dynamics simulations. The radius of gyration reflects the embodied compactness and can reflect the degree of compactness of the system. The above figure shows the variation of RoG with time for six complex systems during molecular dynamics simulation, and the size of the fluctuation can be very intuitively judged from the degree of densification or the convergence of the system

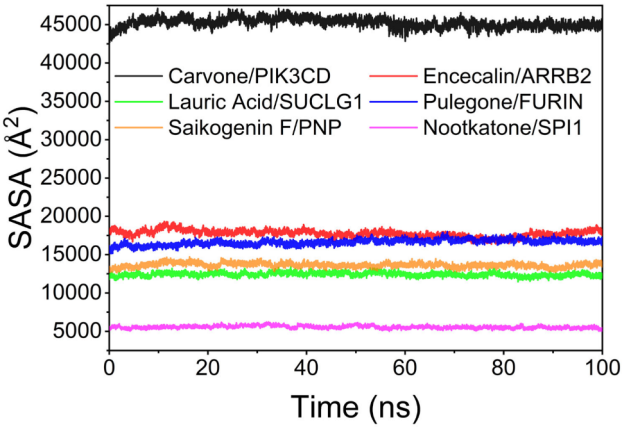

Fig. 14 Solvent accessible surface area (SASA) of individual complexes during molecular dynamics simulations. Based on the fluctuation analysis of SASA, we can see that the fluctuation of the six systems of Carvone-PIK3CD, Encecalin-ARRB2, Lauric Acid-SUCLG1, Pulegone-FURIN, Saikogenin F-PNP, and Nootkatone-SPI1 is smooth, which indicates that the complexes' exposed and buried regions of the surface undergo little change, and the complexes are stable in aqueous solution, providing a basis for the relative stability of small molecules and proteins

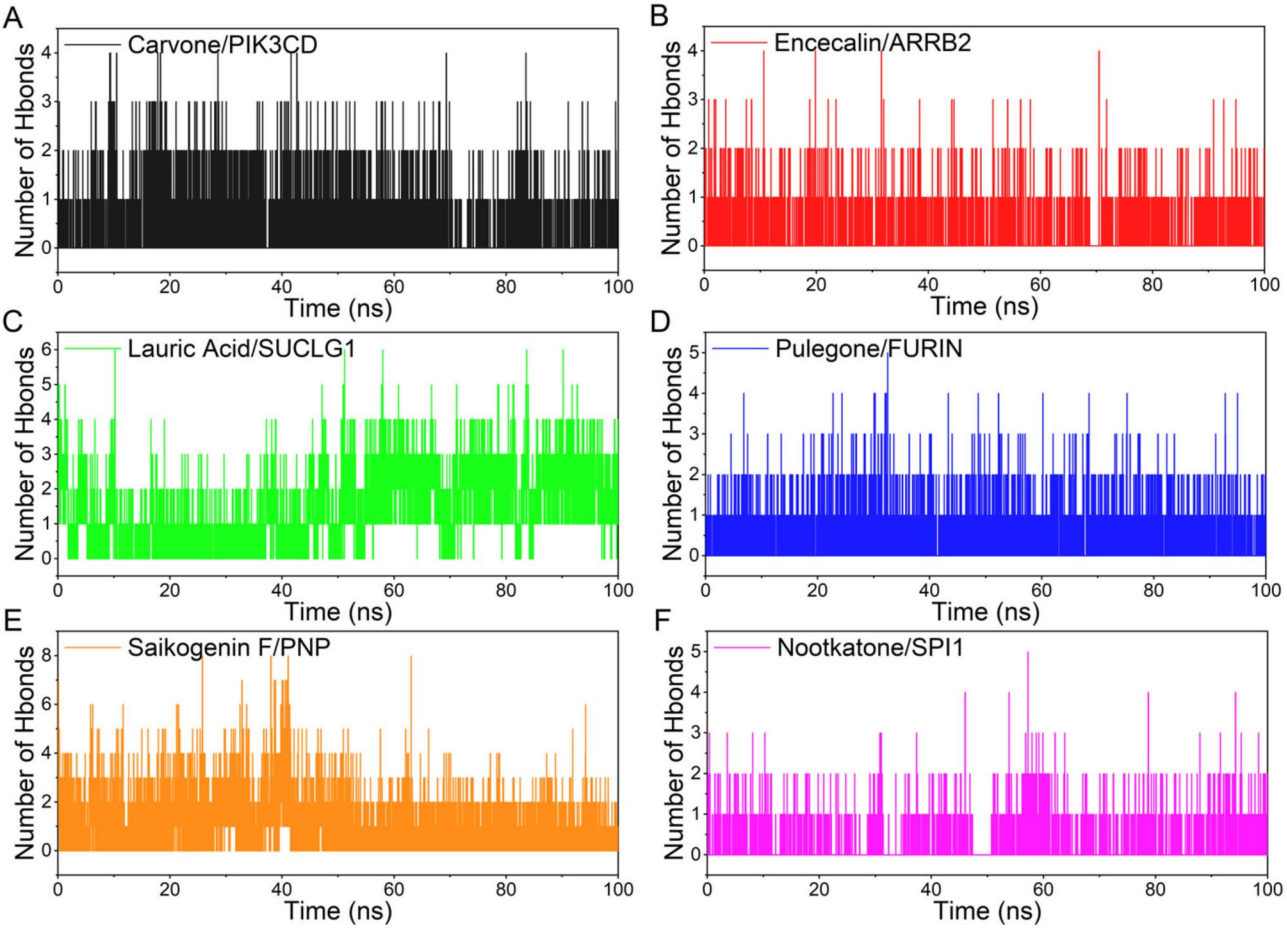

Fig. 15 Change in the number of hydrogen bonds between small molecules and proteins during molecular dynamics simulations. Hydrogen bonding is one of the strongest non-covalent binding interactions, and a higher number indicates better binding

Conclusion

Carvone, Encecalin, Lauric Acid, Pulegone, Nootkatone, and Saikogenin F exhibit the potential to improve survival outcomes and confer antimicrobial characteristics in individuals with sepsis.

Acknowledgements
Not applicable.

Author contributions
H.W and W.X assisted with data analysis and paper writing, Y.L and L.H drew pictures and tables, and Y.H and W.Z were responsible for the final review of the article.

Funding
Funding supported by the Key Clinical Specialty Construction Project in Sichuan Province.

Data availability
The CNGBdb repository contains the datasets that were analyzed for this study, (https://db.cngb.org/search/project/CNP0002611/).

Declarations

Ethics approval and consent to participate
Each patient and their family members voluntarily participated in this study and signed an informed consent form.Approval for the study was granted by the Ethics Committee at the Affiliated Hospital of Southwest Medical University (No.1. ky2018029), Clinical Trial No: ChiCTR1900021261,Registration Date: February 4, 2019.

Consent for publication
Not applicable.

Disclosure
The authors declare no conflicting interests in this study.

Competing interests
The authors declare no competing interests.

Author details
[1]Clinical Medical College, Southwest Medical University, Luzhou, People's Republic of China
[2]Department of Emergency Medicine, The Affiliated Hospital of Southwest Medical University, Luzhou, People's Republic of China

Received: 28 February 2024 / Accepted: 9 September 2024
Published online: 01 October 2024

References

1. Singer M, Deutschman CS, Seymour CW, Shankar-Hari M, Annane D, Bauer M, Bellomo R, Bernard GR, Chiche J, Coopersmith CM, et al. The Third International Consensus definitions for Sepsis and septic shock (Sepsis-3). JAMA-J AM MED ASSOC. 2016;315(8):801.

2. Huang M, Cai S, Su J. The pathogenesis of Sepsis and potential therapeutic targets. INT J MOL SCI. 2019;20(21):5367.
3. Zhao GZ, Guo YH, Li B, Hu J, Chen TF, Di HR, Shao F, Liu QQ. Research progress of traditional Chinese medicine in prevention and treatment of sepsis. Zhongguo Zhong Yao Za Zhi. 2017;42(8):1423–9.
4. Sun P, Li Y, Wei S, Zhao T, Wang Y, Song C, Xue L, Wang F, Xiao L, Wu J, et al. Pharmacological effects and Chemical constituents of Bupleurum. MINI-REV MED CHEM. 2019;19(1):34–55.
5. Yang F, Dong X, Yin X, Wang W, You L, Ni J. Radix Bupleuri: a review of traditional uses, Botany, Phytochemistry, Pharmacology, and Toxicology. BIOMED RES INT. 2017;2017:7597596.
6. Liu ZH, Sun XB. Network pharmacology: new opportunity for the modernization of traditional Chinese medicine. Yao Xue Xue Bao. 2012;47(6):696–703.
7. Hao DC, Xiao PG. Network pharmacology: a Rosetta Stone for traditional Chinese medicine. DRUG DEVELOP RES. 2014;75(5):299–312.
8. Ge SX, Son EW, Yao R. iDEP: an integrated web application for differential expression and pathway analysis of RNA-Seq data. BMC Bioinformatics. 2018;19(1):524–34.
9. Kong X, Liu C, Zhang Z, Cheng M, Mei Z, Li X, et al. BATMAN-TCM 2.0: an enhanced integrative database for known and predicted interactions between traditional Chinese medicine ingredients and target proteins. NUCLEIC ACIDS RES. 2023;52(D1):D1110–D1120.
10. Szklarczyk D, Gable AL, Nastou KC, Lyon D, Kirsch R, Pyysalo S, Doncheva NT, Legeay M, Fang T, Bork P, et al. The STRING database in 2021: customizable protein–protein networks, and functional characterization of user-uploaded gene/measurement sets. NUCLEIC ACIDS RES. 2021;49(D1):D605–12.
11. Zhou Y, Zhou B, Pache L, Chang M, Khodabakhshi AH, Tanaseichuk O, Benner C, Chanda SK. Metascape provides a biologist-oriented resource for the analysis of systems-level datasets. NAT COMMUN. 2019;10(1):1523.
12. Scicluna BP, Klein KP, van Vught LA, Wiewel MA, Ong DS, Zwinderman AH, Franitza M, Toliat MR, Nürnberg P, Hoogendijk AJ, et al. A molecular biomarker to diagnose community-acquired pneumonia on intensive care unit admission. AM J RESP CRIT CARE. 2015;192(7):826–35.
13. Wang C, Li S, Shen Y, Li Y, Chen M, Wang Y, Lan Y, Hu Y. Mechanisms of Panax Ginseng on treating Sepsis by RNA-Seq technology. INFECT DRUG RESIST. 2022;15:7667–78.
14. Wang Y, Xiao J, Suzek TO, Zhang J, Wang J, Zhou Z, Han L, Karapetyan K, Dracheva S, Shoemaker BA, et al. PubChem's BioAssay Database. NUCLEIC ACIDS RES. 2012;40(D1):D400–12.
15. Berman H, Henrick K, Nakamura H. Announcing the worldwide Protein Data Bank. NAT STRUCT MOL BIOL. 2003;10(12):980.
16. Riniker S. Fixed-charge Atomistic Force Fields for Molecular Dynamics Simulations in the condensed phase: an overview. J CHEM INF MODEL. 2018;58(3):565–78.
17. Sagui C, Darden TA. Molecular dynamics simulations of biomolecules: long-range electrostatic effects. Annu Rev Biophys Biomol Struct. 1999;28:155–79.
18. Larini L, Mannella R, Leporini D. Langevin stabilization of molecular-dynamics simulations of polymers by means of quasisymplectic algorithms. J CHEM PHYS. 2007;126(10):104101.
19. Hsin K, Ghosh S, Kitano H. Combining machine Learning systems and multiple docking Simulation packages to improve docking prediction reliability for Network Pharmacology. PLoS ONE. 2014;8(12):e83922.
20. Kempker JA, Martin GS. A global accounting of sepsis. Lancet. 2020;395(10219):168–70.
21. Song Y, Lin W, Zhu W. Traditional Chinese medicine for treatment of sepsis and related multi-organ injury. FRONT PHARMACOL. 2023;14:1003658.
22. Chen X, Zhang J, Xia L, Wang L, Li H, Liu H, Zhou J, Feng Z, Jin H, Yang J, et al. β-Arrestin-2 attenuates hepatic ischemia-reperfusion injury by activating PI3K/Akt signaling. Aging. 2020;13(2):2251–63.
23. Yang X, Zhou G, Ren T, Li H, Zhang Y, Yin D, Qian H, Li Q. β-Arrestin prevents cell apoptosis through pro-apoptotic ERK1/2 and p38 MAPKs and anti-apoptotic akt pathways. Apoptosis. 2012;17(9):1019–26.
24. Wang X, Huang G, Mu J, Cong Z, Chen S, Fu D, Qi J, Li Z. Arrb2 promotes endothelial progenitor cell-mediated postischemic neovascularization. THERANOSTICS. 2020;10(21):9899–912.
25. Zhang Y, Gao X, Bai X, Yao S, Chang YZ, Gao G. The emerging role of furin in neurodegenerative and neuropsychiatric diseases. TRANSL NEURODEGENER. 2022;11(1):39.
26. Douglas L, Reihill JA, Montgomery BM, Martin SL. Furin as a therapeutic target in cystic fibrosis airways disease. EUR RESPIR REV. 2023;32(168):220256.
27. Vong L. Gene therapy for PNP deficiency protocol. LymphoSign J. 2018;5(3):115–20.
28. Davenne T, Rehwinkel J. PNP inhibitors selectively kill cancer cells lacking SAMHD1. MOL CELL ONCOL. 2020;7(6):1804308.
29. El-Hattab AW, Craigen WJ, Scaglia F. Mitochondrial DNA maintenance defects. BBA-MOL BASIS DIS. 2017;1863(6):1539–55.
30. Molaei RS, Erfanian OM, Tabasinezhad M, Alipoor B, Salmani TA, Ghaedi H. SUCLG1 mutations and mitochondrial encephalomyopathy: a case study and review of the literature. MOL BIOL REP. 2020;47(12):9699–714.
31. Johansen KH, Golec DP, Thomsen JH, Schwartzberg PL, Okkenhaug K. PI3K in T cell adhesion and trafficking. FRONT IMMUNOL. 2021;12:708908.
32. Bier J, Deenick EK. The role of dysregulated PI3Kdelta signaling in human autoimmunity. IMMUNOL REV. 2022;307(1):134–44.
33. Prange KH, Singh AA, Martens JH. The genome-wide molecular signature of transcription factors in leukemia. EXP HEMATOL. 2014;42(8):637–50.
34. Zhang G, Lu J, Zheng J, Mei S, Li H, Zhang X, Ping A, Gao S, Fang Y, Yu J. Spi1 regulates the microglial/macrophage inflammatory response via the PI3K/AKT/mTOR signaling pathway after intracerebral hemorrhage. NEURAL REGEN RES. 2024;19(1):161–70.
35. Xie W, Zou S, Dong C, Yang C. SPI1-mediated autophagy of peripheral blood monocyte cells as a mechanism for sepsis based on single-cell RNA sequencing. INT IMMUNOPHARMACOL. 2023;117:109909.
36. Yang Q, Luo J, Lv H, Wen T, Shi B, Liu X, Zeng N. Pulegone inhibits inflammation via suppression of NLRP3 inflammasome and reducing cytokine production in mice. IMMUNOPHARM IMMUNOT. 2019;41(3):420–7.
37. Shi L, Tu YJ, Ye SQ, Xia Y, Ma CZ, Peng XZ, Liu YW, Ai ZZ, You PT. A potential anti-cancer compound separated from the Chloroform Extract of the Chinese Medicine Formula Shenqi San. CURR MED SCI. 2020;40(1):138–44.
38. Tham YY, Choo QC, Muhammad T, Chew CH. Lauric acid alleviates insulin resistance by improving mitochondrial biogenesis in THP-1 macrophages. MOL BIOL REP. 2020;47(12):9595–607.
39. Asle-Rousta M, Amini R, Aghazadeh S. Carvone suppresses oxidative stress and inflammation in the liver of immobilised rats. ARCH PHYSIOL BIOCHEM. 2023;129(3):597–602.
40. Gai Y, Bai C, Zhang W, Xiao H, Xu J, Hou J, Ge X. Nootkatone attenuates airway inflammation in asthmatic mice through repressing ROS-induced NLRP3 inflammasome activation. BIOCHEM CELL BIOL. 2023;101(6):513–22.
41. Romero-Cerecero O, Islas-Garduño AL, Zamilpa A, Tortoriello J. Effectiveness of an encecalin standardized extract of Ageratina pichinchensis on the treatment of onychomycosis in patients with diabetes mellitus. PHYTOTHER RES. 2020;34(7):1678–86.

Publisher's note